Piezoelectricity and charge trapping in ZnO and Co-doped ZnO thin films

Domenico D'Agostino, Cinzia Di Giorgio, Antonio Di Trolio, Anita Guarino, Anna Maria Cucolo, Antonio Vecchione, and Fabrizio Bobba

Citation: AIP Advances **7**, 055010 (2017); doi: 10.1063/1.4983474
View online: http://dx.doi.org/10.1063/1.4983474
View Table of Contents: http://aip.scitation.org/toc/adv/7/5
Published by the American Institute of Physics

AIP ADVANCES 7, 055010 (2017)

Piezoelectricity and charge trapping in ZnO and Co-doped ZnO thin films

Domenico D'Agostino,[1] Cinzia Di Giorgio,[1] Antonio Di Trolio,[2] Anita Guarino,[1] Anna Maria Cucolo,[1,3] Antonio Vecchione,[3] and Fabrizio Bobba[1,3,a]
[1]*Physics Department "E.R. Caianiello," University of Salerno, Fisciano, Salerno, Italy*
[2]*CNR-Istituto dei Sistemi Complessi, U.O.S. di Tor Vergata, Roma, Italy*
[3]*CNR-SPIN Salerno, Fisciano, Salerno, Italy*

(Received 13 February 2017; accepted 26 April 2017; published online 17 May 2017)

Piezoelectricity and charge storage of undoped and Co-doped ZnO thin films were investigated by means of PiezoResponse Force Microscopy and Kelvin Probe Force Microscopy. We found that Co-doped ZnO exhibits a large piezoelectric response, with the mean value of piezoelectric matrix element d_{33} slightly lower than in the undoped sample. Moreover, we demonstrate that Co-doping affects the homogeneity of the piezoelectric response, probably as a consequence of the lower crystalline degree exhibited by the doped samples. We also investigate the nature of the interface between a metal electrode, made up of the PtIr AFM tip, and the films as well as the phenomenon of charge storage. We find Schottky contacts in both cases, with a barrier value higher in PtIr/ZnO than in PtIr/Co-doped ZnO, indicating an increase in the work function due to Co-doping. [http://dx.doi.org/10.1063/1.4983474]

I. INTRODUCTION

Zinc Oxide (ZnO) is a well-known wide-bandgap (3.4eV) metal oxide semiconductor which has been attracting the interest of the scientific community for several decades. More recently, there has been renewed interest in it due to improvements in epitaxial growth techniques as well as in the fabrication of micro- and nano-structures,[1–5] and due to the possibility of p-type conductivity[6] and ferromagnetic behavior[7] as a consequence of cation doping. In addition to this, as it shows much stronger electric polarization effects than other wide-gap semiconductors, such as GaN and SiC,[8,9] ZnO has great potential for manufacturing energy-harvesting systems.[2,10–12] Moreover, as ZnO is a semiconducting piezoelectric material, it is already widely used in microelectromechanical systems for making sensors[13] and actuators[14] and in communications for surface acoustic wave and thin film bulk acoustic wave resonator devices.[15,16] However, ZnO's piezoelectric response is affected by its built-in electric field, due to the high mobility of its charge carriers, which might partially compensate the effect of an external applied electric field.[17] The control of ZnO conductivity by means of extrinsic doping can thus lead to a fine tuning of the piezoelectricity, which may also provide it with ferroelectric responses, whereas the ferroelectricity of undoped ZnO has never been reported from experiments on a macroscopic scale.[17] By contrast, local ferroelectricity can be induced by the presence of Li and Cu doping[18–21] as well as polar defects such as O vacancies at the surface,[22–24] and can be probed by performing experiments at the nanoscale.

Several techniques, including scanning probe microscopy-based experiments, have been employed to study the polarization of undoped and doped ZnO thin films at the nanoscale as well as ZnO one-dimensional structures. However, even though 1D nanostructures are attractive for fundamental research studies, their lack of reproducibility still affects their industrial application, whereas the well-consolidated thin film technology guarantees greater success.

[a]fbobba@unisa.it; Tel.: +39-089-969-490

The main goal of our work was to investigate the polarization and charge-storage possibility of undoped and Co-doped ZnO thin films by means of PiezoResponse Force Microscopy (PFM) and Kelvin Probe Force Microscopy (KPFM) experiments. By doing this, we gained insights into the charge-injection mechanism as well as into the role of polar defects at the metal/semiconducting interface.

Originally used to detect domain structures, polarization switching, and for local hysteresis spectroscopy in ferroelectric materials,[25–27] PFM has recently been extended to characterize piezoelectric semiconductors, such as GaN, AlN, and ZnO.[28–31] Indeed, recently several PFM investigations on ZnO nanostructures and thin films have been carried out.[32–35] Here, we present PFM experiments on both undoped and Co-doped ZnO thin films, aiming at investigating the spatial distribution of the out-of-plane piezoelectric matrix element d_{33}, which measures the material displacement in the same direction as the applied out-of-plane electric field. Moreover, we present a qualitative understanding of the surface polarization by studying the phase of the piezoelectric response with respect to an AC external bias. On the other hand, KPFM experiments will be presented below with the aim of studying the charging phenomenon at the metal/semiconducting ZnO or Co-doped ZnO interface. Indeed, KPFM is a well-established technique that has been used to measure the contact potential between two surfaces brought into close proximity with each other.[36–39] By doing this, we will be able to qualify the nature of the interface between the metal electrode (atomic force microscopy tip) and our samples as a Schottky barrier and we will investigate the phenomenon of charge storage in both ZnO and Co-doped ZnO.[40,41]

II. RESULTS

A. Sample characterization

ZnO and $Zn_{0.95}Co_{0.05}O$ films of 50nm in thickness were deposited by pulsed laser deposition and preliminarily characterized by X-ray diffraction (XRD) and energy-dispersive X-ray spectroscopy (EDS) analyses. The structure and crystallographic orientation of ZnO and $Zn_{0.95}Co_{0.05}O$ films were investigated by XRD using the Cu Kα line (λ = 1.5418 Å) and, as reported elsewhere,[42] the results of the analysis confirm the formation of an expected wurtzite structure. Here, a scanning electron microscope equipped with an energy-dispersive spectrometer (EDS), Oxford INCA Energy 300, used for overall microstructural and compositional analysis on both ZnO and $Zn_{0.95}Co_{0.05}O$ samples is presented. The spectra in Fig. 1, acquired on a large area of the films (about 2mm × 1mm in size), are representative of the undoped (in black) and Co-doped materials (in red). As expected Zn, O, Co and Si peaks appear in the spectra, while a C contamination was additionally measured on both samples, due to their exposure to the air after fabrication. The Co content of the doped film was measured by averaging several analyses performed on many different areas of the samples, each about 200μm × 100μm in size, mainly resulting in a Co/Zn ratio slightly higher than 5% (about 6%), which reasonably agrees with the nominal composition. A slight excess of Co was detected only at the edges of the sample.

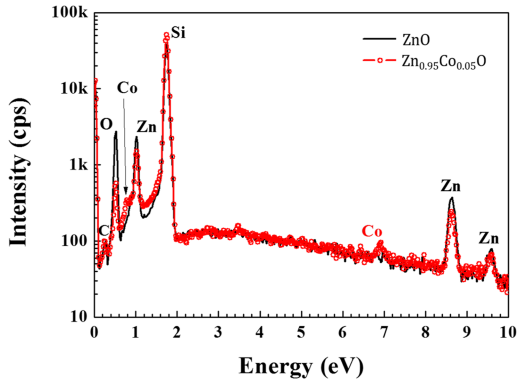

FIG. 1. EDS analysis of ZnO (in black) and $Zn_{0.95}Co_{0.05}O$ (in red).

B. Piezoelectricity

The local electromechanical response of both undoped and doped ZnO was investigated at the nanoscale by means of scanning probe microscopy-based experiments, such as PiezoResponse Force Microscopy (PFM). Fig. 2 shows the topography and piezoelectric response of both ZnO and $Zn_{0.95}Co_{0.05}O$ samples. Fig. 2(a) and (d) are representative maps for ZnO and $Zn_{0.95}Co_{0.05}O$ morphology on a scan area measuring 3μm × 3μm. Among all the measured areas, a clear difference appears between the two samples: ZnO exhibits crystallites with almost regular shape and sharp edges, though with an incoherent orientation. On the other hand, $Zn_{0.95}Co_{0.05}O$ shows a granular topography in which single grains as well as more extended clusters of grains are recognizable. In particular, a small number of bigger grains and clusters measuring hundreds of nm in height and lateral size lie on a carpet of small $Zn_{0.95}Co_{0.05}O$ grains measuring a few tenths of a nm. Such a value might be affected by a systematic error due to the finite tip resolution, determined by its minimum nominal radius of 10nm. Whenever the size of the tip becomes comparable to or bigger than the grain size, an overestimate will affect the measurements. Fig. 2(g) presents the roughness distribution of a surface in ZnO (in red) and $Zn_{0.95}Co_{0.05}O$ (in blue). ZnO shows lower roughness and sharper distribution, centered around 20nm, whereas $Zn_{0.95}Co_{0.05}O$ presents a much wider distribution centered around 60nm. Our results correlate well with previous works where a reduction in material crystallinity was proved to occur after Co-doping.[41]

Amplitude and phase maps of the piezoelectric response to the external AC bias are presented in Fig. 2(b)–(c) for ZnO and Fig. 2(e)–(f) for $Zn_{0.95}Co_{0.05}O$. While the PFM amplitude provides information on the magnitude of the electromechanical displacements, the PFM phase depends on

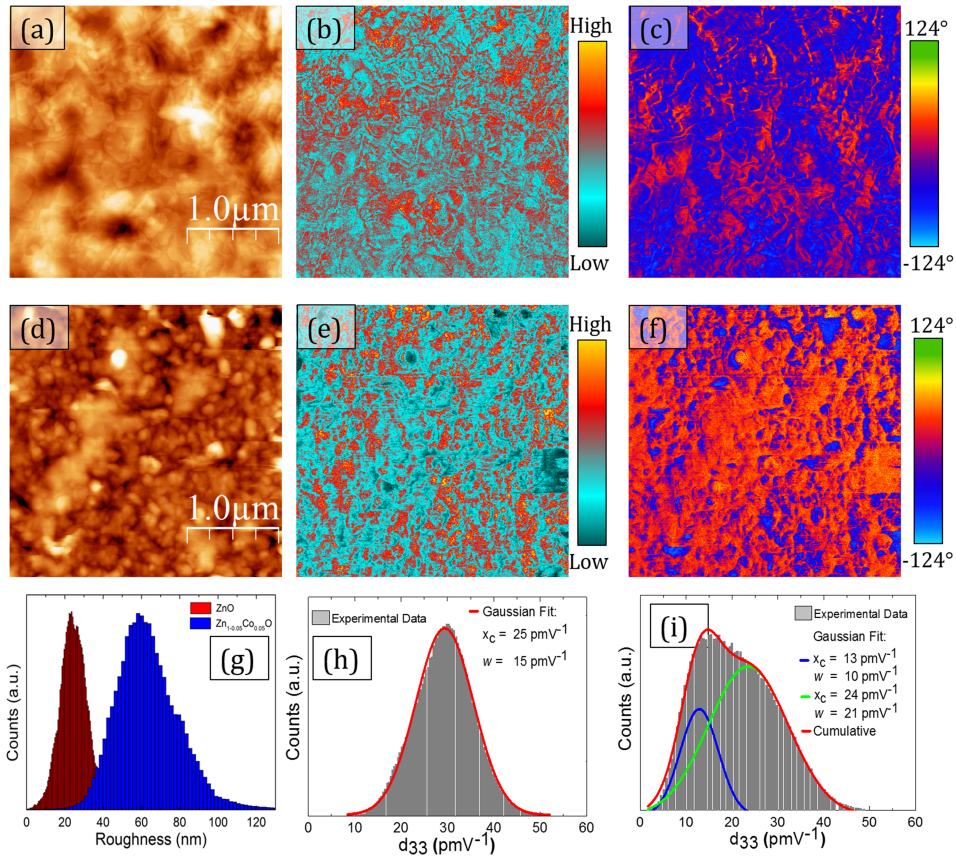

FIG. 2. (a) Topography, (b) PFM amplitude and (c) PFM phase acquired on a 3μm × 3μm scan area of ZnO sample. (d) Topography, (e) PFM amplitude and (f) PFM phase acquired on a 3μm × 3μm scan area of $Zn_{0.95}Co_{0.05}O$ sample. The topographies were acquired in contact mode by applying a constant pressure of 10nN. PFM amplitude and phase were acquired by applying an external AC bias having V_{AC}=500mV and f=50kHz. (g) Roughness Analysis of (a) in red and (b) in blue. (h)-(i) Spatial distribution of d_{33} for ZnO and $Zn_{0.95}Co_{0.05}O$, respectively.

the polarity of the piezoelectric domains. In the case of ZnO, it is well known that, for perfectly c-axis-oriented films, local spontaneous polarization orientation is either from the top surface to the bottom electrode or vice-versa, depending on the terminating atom at the surface.[33] Indeed, a spontaneous polarization is driven by the presence of ions at the surface (the polar surface is positively charged when terminating with Zn(0001) and negatively charged when terminating with O(0001)) and always points from the Zn face to the O face. For perfectly c-axis-oriented ZnO films, the PFM phase image is then either in-phase or out-of-phase with the external AC driving voltage, corresponding to a Zn- or O-terminating surface, respectively. This allows the determination of the spontaneous polarization as well as the crystalline orientation of the material by studying PFM phase images.

Figs. 2(b) and 2(e) show the amplitude maps for the piezoelectric signals for ZnO and $Zn_{0.95}Co_{0.05}O$, respectively. Here, regions with higher piezoelectricity (red/yellow in the color scale used) are clearly recognizable in the maps. We do not observe any strong correspondence between morphological and piezoelectric features in ZnO, while in $Zn_{0.95}Co_{0.05}O$ the highest grains seem to contribute with a lower piezoelectric displacement. In addition to this, the histograms in Fig. 2(h)–(i) detail the distribution of the out-of-plane piezoelectric matrix element d_{33} for ZnO and $Zn_{0.95}Co_{0.05}O$, respectively. Its values were calculated by rescaling the amplitude maps with respect to both the applied voltage V_{ac} and the quality factor Q of the resonance peak at the working frequency (V_{ac}=500mV at f=50kHz and Q=20-30 in the presented measurements), $d_{33} = \frac{Amplitude[nm]}{V_{ac}[V]Q}$. As shown in Fig. 2(h), the d_{33} distribution of ZnO is well fitted by a single-peak Gaussian function having a mean value of 25pmV^{-1} and a standard deviation of 15pmV^{-1}. This value is in good agreement with previous d_{33} measurements on the same material.[32–35] On the other hand, the d_{33} distribution of $Zn_{0.95}Co_{0.05}O$, in Fig. 2(i) is much wider and may be fitted by a double-peak Gaussian function centered around 13pmV^{-1}, with a standard deviation of 10pmV^{-1}, and 24pmV^{-1} with a standard deviation of 21pmV^{-1}. By comparing these results, we infer that Co-doping reduces the homogeneity of the piezoelectric response with respect to the pure sample. However, at this stage we cannot discriminate if this is due to an intrinsic property of the Co-doped material rather than to its reduced crystal growth quality.

On the other hand, the piezoelectric phase response of both samples (Figs. 2(c) and 2(f) for ZnO and $Zn_{0.95}Co_{0.05}O$, respectively) do not show a coherent orientation of the grain polarization. Indeed, a net phase shift of 45° and 98° is measured for ZnO and $Zn_{0.95}Co_{0.05}O$, respectively, across the scanned area. However, by using the same phase contrast ranges in Figs. 2(c) and 2(f), the piezoelectric responses of each map can be easily compared. Since the polarization is never completely out-of-phase with respect to the external AC bias (the measured phase is never 180°), we can infer the absence of O-terminating polar surfaces in both samples. On the other hand, ZnO shows a bigger portion of the map where the value of the piezoelectric phase is 0° (purple regions in Fig. 2(c)), corresponding to the presence of Zn-terminating atoms. In contrast, $Zn_{0.95}Co_{0.05}O$ almost never oscillates in-phase with the external AC bias (most of the phase map is either blue or orange, corresponding to negative or positive 50°). We speculate that such a difference is driven by the reduced crystallinity of $Zn_{0.95}Co_{0.05}O$, which leads to the absence of a polar surface.

C. Metal/semiconductor interface and charge trapping

In order to investigate the distribution of contact potential difference V_{CPD} between a metallic electrode (the tip) and undoped or doped ZnO, Kelvin Probe Force Microscopy (KPFM) experiments were performed. Figs. 3(a)–(b) show V_{CPD} maps for a PtIr tip and both ZnO and $Zn_{0.95}Co_{0.05}O$ on regions of 3μm × 3μm in size. In the color scale used, bright areas indicate regions with higher contact potential than dark ones. We did not observe any clear correlation between topography and potential maps in the ZnO sample (Fig. 3(a)), while the V_{CPD} maps for $Zn_{0.95}Co_{0.05}O$ (Fig. 3(b)) show the features of a granular morphology. Such a direct convolution of the topography with the electrostatic interaction is caused by the intrinsic surface potential distribution of the $Zn_{0.95}Co_{0.05}O$ grains rather than by a spurious cross-talk artefact affecting the apparatus. Indeed, by using a lift height of 150nm, the short-range Van der Waals forces cannot play any role during V_{CPD} acquisition. By taking into account the following definition of work function for a semiconductor, $W = \chi + (E_c - E_F) + qV$, where χ is the electron affinity, $(E_c - E_F)$ is the energy difference between the minimum of the conductance band and the Fermi level, and qV is the surface band bending, we infer that the high

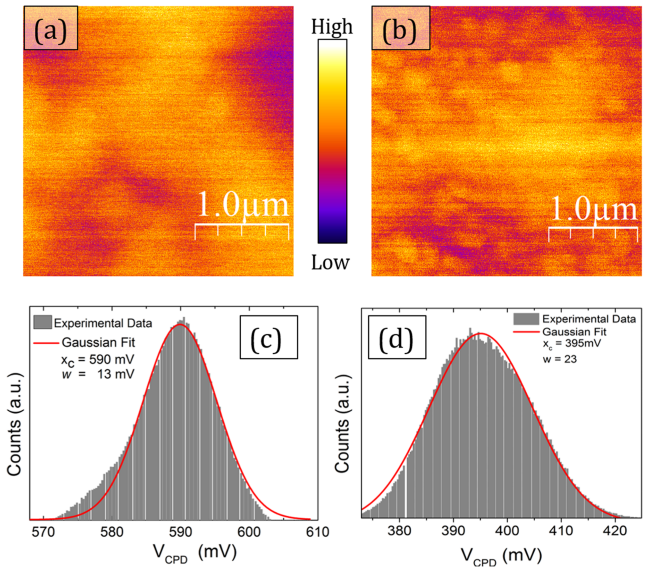

FIG. 3. Contact potential difference maps for (a) ZnO and (b) $Zn_{0.95}Co_{0.05}O$ acquired on a scan area of 3μm × 3μm in size. The driving AC voltage and the lift height were chosen as V_{ac}=700mVsin(80kHz*t) and h=100nm in (a) and V_{ac}=550mVsin(80kHz*t) and h=150nm in (b). (c)-(d) Contact potential difference distribution for ZnO and $Zn_{0.95}Co_{0.05}O$, respectively. Superimposed on the distributions, in red, are the fits of the experimental data.

correspondence between contact potential and topographic granularity may be related to the presence of charges trapped on the surface of each grain, affecting both the Fermi level position as well as the band banding.

In addition to this, the V_{CPD} distributions of ZnO and $Zn_{0.95}Co_{0.05}O$ are reported in Figs. 3(c)–(d), respectively. In both cases, a single-peak Gaussian function fits the experimental data well, indicating that a mean contact potential difference of 590mV (395mV) is established between the tip and the ZnO ($Zn_{0.95}Co_{0.05}O$). However, a higher uniformity of V_{CPD} is measured on the ZnO surface with respect to $Zn_{0.95}Co_{0.05}O$, which is reflected by the standard deviations of the fits, resulting in 13mV and 23mV, respectively. We underline that, in both cases, the measured contact potential difference is positive, resulting from $W_{tip}>W_{sample}$, which allows us to qualify both the PtIr/ZnO and PtIr/$Zn_{0.95}Co_{0.05}O$ interfaces as Schottky barriers. Moreover, the decrease in V_{CPD} in the presence of Co-doping indicates that the $W_{Zn0.95Co0.05O}$ rises by ~200meV with respect to W_{ZnO}, due to the lower values of the carrier concentration and hence of the shift of the Fermi level towards the valence band.[43]

III. DISCUSSION

In this work, the converse piezoelectric effect and the charge storage phenomenon in undoped and Co-doped ZnO thin films were investigated at the nanoscale by means of PiezoResponse Force Microscopy (PFM) and Kelvin Probe Force Microscopy (KPFM). The first clear difference between ZnO and $Zn_{0.95}Co_{0.05}O$ arises from morphological analyses, which show a reduction in crystallinity in the case of the doped sample. This confirms previous results, where the addition of Co to ZnO was shown to favor more disordered growth.[41] By performing PFM experiments, we estimated the spatial distribution of the out-of-plane piezoelectric matrix element d_{33} on a surface area of 3μm × 3μm in size on both ZnO and $Zn_{0.95}Co_{0.05}O$. In the first case, a sharper d_{33} distribution was found, with a mean value of 25±15 pmV^{-1}, whereas a less uniform d_{33} distribution, showing two distinct mean values, respectively of 13±10pm^{-1} and 24±21pm^{-1}, is measured on the doped sample. We infer that the lower homogeneity in the piezoelectric properties of $Zn_{0.95}Co_{0.05}O$ well accords with its reduced crystallinity. Indeed, the d_{33} estimate of ZnO is in good agreement with values reported in literature.[33–35] On the other hand, the PFM phase images show a maximum phase shift of 45° and 98° in ZnO and $Zn_{0.95}Co_{0.05}O$, respectively. We can thus conclude that the piezoelectric

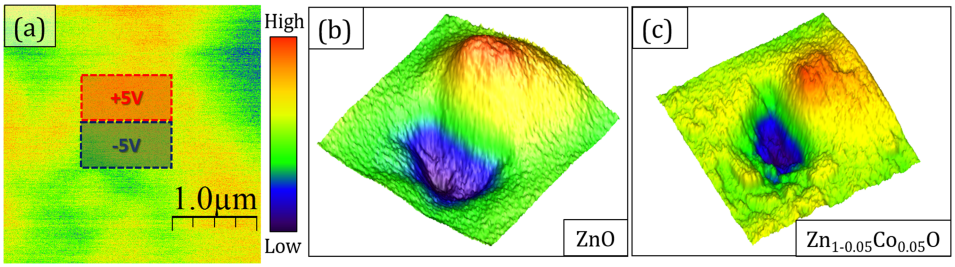

FIG. 4. (a) sketch of the charging procedure: negative and positive DC bias is subsequently applied on a 1μm × 1μm scan area. KPFM maps acquired on ZnO (b) with V_{ac}=700mVsin(80kHz*t) and h=100nm and $Zn_{0.95}Co_{0.05}O$ (c) with V_{ac}=550mVsin(80kHz*t) and h=100nm. Both areas are 3μm × 3μm in size.

displacements of ZnO have a higher tendency to oscillate in-phase with the external AC bias than $Zn_{0.95}Co_{0.05}O$. In addition, no 180°-phase shift was measured in any of the scanned regions on both undoped and doped samples. The observed piezoelectrical response can be explained by taking into account the electrical polarization, that is expected in ZnO and ZnO-based materials, together with either a charge-injection or charge-induction mechanism at the metallic tip-sample interface. KPFM experiments were performed on both ZnO and $Zn_{0.95}Co_{0.05}O$, in order to discriminate between these two possibilities. Indeed, as the contact potential difference V_{CPD} is always positive, a Schottky barrier rather than an Ohmic contact is expected at both the PtIr/ZnO and PtIr/$Zn_{0.95}Co_{0.05}O$ interfaces, which should strongly inhibit the charge-injection phenomenon. Moreover, the V_{CPD} of $Zn_{0.95}Co_{0.05}O$ is reduced by ~200mV compared to ZnO, resulting from the increase of the work function after Co-doping, which indicates only a small reduction in the Schottky barrier. In addition to this, the charge-injection mechanism is not compatible with the results of the charge-storage experiments presented in Fig. 4. Indeed, if charge carriers were injected across the tip/sample interface, we would expect an inverted contrast in the KPFM signal when imaging regions previously poled with positive or negative 5V. We can thus infer that only charge induction and electrical polarization play a role in the charge-storage phenomenon measured on our samples.

IV. MATERIALS AND METHODS

Thin ZnO and $Zn_{0.95}Co_{0.05}O$ films were deposited by pulsed laser deposition using a Nd:YAG laser operating at λ = 355 nm (fluence ~ 2 J/cm^2) with 7 nm of pulse duration and 10 Hz of repetition rate, starting from $Zn_{1-x}Co_xO$ pellets with nominal Co contents of x = 0, and 0.05. The samples were grown on highly p-doped Si(100) single crystals, working as bottom electrode during the scanning probe microscopy experiments. Thickness and resistivity of Si(100) substrates were 0.5mm and 0.001-0.01 Ohm×cm, respectively. Before being loaded in the deposition chamber, the Si crystals were ultrasonicated in acetone and ethanol. Once in the chamber, the substrates were degassed by heating them up to about 500°C, where those were kept for about 15 min (P=10^{-6} mbar). During the deposition, substrate-target distance, substrate temperature and O_2 pressure were 5cm, 480 °C and 2×10^{-5} mbar, respectively. In these conditions, taking into account the duration time of 110 s and the typical rate of the deposition of ~0.4 nm/sec, we estimated a thickness of about 50nm for both materials. The ϑ-2ϑ X-ray diffraction pattern of both ZnO and $Zn_{0.95}Co_{0.05}O$ shows a peak at about 34.5°, characteristic of the (002) reflection in the ZnO wurzite structure. A sharper and more intense peak is measured in the case of ZnO, indicating a higher crystallinity with respect to the Co-doped sample.

All the scanning probe microscopy measurements were performed using a Multimode AFM with Nanoscope V controller, inside a glove box kept at %RH=30 by flowing N_2 gas.

In PFM mode, an alternating-current (AC) voltage was applied between a conducting tip at the end of a cantilever and the p-type Si substrate, thus forming an almost perpendicular electric field across the sample. The AFM tip was kept in stable contact on the sample surface by applying a normal force of 10 nN. In the presence of a converse piezoelectric effect, the alternating electric field causes local deformations (expansions and contractions) of the sample. The sample displacements

lead to mechanical oscillations of the cantilever in contact with its surface, that can be measured by the AFM apparatus through a standard lock-in amplifier. Amplitude and phase of such oscillations with respect to the driving AC voltage are thus acquired during the PFM experiments. In this study, a Si tip covered by Platinum-Iridium (SCM-PIC from Bruker) with a resonance frequency of 11.5 kHz and spring constant of 0.4 N/m was used. An AC voltage with magnitude of 500 mV and frequency of 50kHz was applied between the conductive tip and the sample. Indeed, so-called single-frequency PFM was employed to acquire the vertical displacement, where 50kHz is the characteristic resonance frequency of the tip-sample contact. By doing this, the quality factor Q of the resonance peak works as a magnifying factor, enhancing the piezoelectric response. Once Q is known from the contact resonance curve and the photodiode response is calibrated through the tip-sample force-distance curve, the out-of-plane coefficient of the piezoelectric matrix can be extracted from the amplitude maps, by exploiting the following relation: $d_{33} = \frac{Amplitude[nm]}{V_{ac}[V]Q}$.

On the other hand, KPFM experiments were employed to study the contact potential difference V_{CPD} between the metallic tip and ZnO ($Zn_{0.95}Co_{0.05}O$) sample and, consequently, the nature of the barrier at the metal/semiconductor interface (Schottky or Ohmic). In general, V_{CPD} is defined as $V_{CPD} = \frac{W_m - W_s}{q}$ where q is the electronic charge, while W_m and W_s are the work functions of metal (tip) and semiconductor (sample), respectively. In KPFM, V_{CPD} is measured by applying at the same time an AC and a DC voltage ($V_{ac} = V_{AC}\sin(\omega t)$ and V_{DC}) to the tip, while it scans in lift mode over the sample surface. Here, the frequency of the AC bias is chosen at the resonance frequency of the cantilever in order to increase the signal-to-noise ratio. The electrostatic force component measured at frequency ω has the following expression: $F_\omega = \frac{dC}{dz}\left[V_{DC} - V_{CPD}\right] V_{AC}\sin(\omega)$, where C is the tip-sample capacitance and z is the tip-sample distance (lift height). It is thus clear that the V_{CPD} can be measured by applying a DC voltage V_{DC} such that the oscillating amplitude at ω is nullified. In this study, a Si tip coated with Platinum-Iridium (SCM-PIT from Bruker) with a resonant frequency of 80 kHz and spring constant of 3 N/m was used, a V_{AC}=500÷700mV was applied and a lift scan height of 100÷150nm was employed in order to investigate the nature of the PtIr/ZnO (PtIr/$Zn_{0.95}Co_{0.05}O$) interface. Indeed, at the metal/semiconducting interface, the nature of the barrier can be strongly modified by the intrinsic and/or extrinsic doping of the semiconductor, which causes the Fermi level to move inside the energy gap. Whenever $W_m\left(W_{tip}\right) > W_{sample}$ (positive V_{CPD} in KPFM measurements), a Schottky barrier is expected at PtIr/ZnO (PtIr/$Zn_{0.95}Co_{0.05}O$); otherwise, an Ohmic contact is predicted.

V. CONCLUSIONS

We performed scanning probe microscopy experiments on PLD-grown ZnO and $Zn_{0.95}Co_{0.05}O$ thin films. We proved a reduction in sample crystallinity after Co-doping, causing an increase in the inhomogeneity of the piezoelectric properties. We measured an increase of about 200meV in the work function of $Zn_{0.95}Co_{0.05}O$ compared to ZnO and we investigated the charge-storage phenomenon in both samples. Our results allowed us to detail the contribution of electrical polarization, charge injection and charge induction at the interface between the metallic AFM tip and our samples.

ACKNOWLEDGMENTS

Work done in Salerno was funded by Università degli Studi di Salerno (FARB_Bobba2014). One of the authors, D.D.A., would like to acknowledge his financial support from MIUR (Ministry of Education, Universities and Research of the Italian Government). We also acknowledge the CNR-ISC Roma and the CNR-SPIN Salerno, for supporting the project and for making laboratory facilities available. We wish to acknowledge A. Amore Bonapasta and P. Alippi (CNR-ISM Roma) for the fruitful discussions and A. Green (University of Bari Aldo Moro) for kindly proofreading the paper.

[1] V. Cauda, P. Motto, D. Perrone, G. Piccinini, and D. Demarchi, Nanoscale Res. Lett. **9**, 53 (2014).
[2] V. F. Rivera, F. Auras, P. Motto, S. Stassi, G. Canavese, E. Celasco, T. Bein, B. Onida, and V. Cauda, Chem. Eur. J. **19**, 14665 (2013).
[3] M. Laurenti, V. Cauda, R. Gazia, M. Fontana, V. F. Rivera, S. Bianco, and G. Canavese, Eur. J. Inorg. Chem. **14**, 2520 (2013).

[4] C. Ottone, K. Bejtka, A. Chiodoni, V. Farias, I. Roppolo, G. Canavese, S. Stassi, and V. Cauda, New J. Chem. **38**, 2058 (2014).
[5] Z. L. Wang, J. Phys. Condens. Matter **16**, R829 (2004).
[6] L. Duan, W. Zhang, W. Yu, P. Wang, Z. Jiang, L. Luan, Y. Chen, and D. Li, Solid State Commun. **157**, 45 (2013).
[7] Y. Zhang, T. Guo, Y. D. Luo, Y. H. Lin, and C. W. Nan, J. Am. Ceram. Soc. **96**, 361 (2013).
[8] F. Bernardini, V. Fiorentini, and D. Vanderbilt, Phys. Rev. B **56**, R10024 (1997).
[9] A. Qteish, V. Heine, and R. J. Needs, Phys. Rev. B **45**, 6376 (1992).
[10] R. Gazia, P. Motto, S. Stassi, A. Sacco, A. Virga, A. Lamberti, and G. Canavese, Nano Energy **2**, 1294 (2013).
[11] S. Stassi, V. Cauda, C. Ottone, A. Chiodoni, C. F. Pirri, and G. Canavese, Nano Energy **13**, 474 (2015).
[12] Z. L. Wang and J. Song, Science **312**, 242 (2006).
[13] E. Comini, G. Faglia, G. Sberveglieri, Z. Pan, and Z. L. Wang, Appl. Phys. Lett. **81**, 1869 (2002).
[14] T. Shibata, K. Unno, E. Makino, Y. Ito, and S. Shimada, Sens. Actuators A: Phys. **102**, 106 (2002).
[15] S. H. Kim, J. S. Lee, H. C. Choi, and Y. H. Lee, IEEE Electron Dev. Lett. **20**, 113 (1999).
[16] Q. X. Su, P. Kirby, E. Komuro, M. Imura, Q. Zhang, and R. Whatmore, IEEE Trans. Microw. Theory Tech. **49**, 769 (2001).
[17] J. Xiao, T. S. Herng, J. Ding, and K. Zeng, Acta Materialia **123**, 394 (2017).
[18] T. S. Herng, M. F. Wong, D. Qi, J. Yi, A. Kumar, A. Huang, F. C. Kartawidjaja, S. Smadici, P. Abbamonte, C. Sánchez-Hanke, S. Shannigrahi, J. M. Xue, J. Wang, Y. P. Feng, A. Rusydi, K. Zeng, and J. Ding, Adv. Mater. **23**, 1635 (2011).
[19] C. W. Zou, H. J. Wang, M. L. Yin, M. Li, C. S. Liu, L. P. Guo, D. J. Fu, and T. W. Kang, J. Cryst. Growth **312**, 906 (2010).
[20] H. Liu, Y. Wang, J. Wu, G. Zhang, and Y. Yan, Phys. Chem. Chem. Phys. **17**, 9098 (2015).
[21] W. L. Ong, H. Huang, J. Xiao, K. Zeng, and G. W. Ho, Nanoscale **6**, 1680 (2014).
[22] T. S. Herng, A. Kumar, C. S. Ong, Y. P. Feng, Y. H. Lu, K. Y. Zeng, and J. Ding, Sci. Rep. **2**, 587 (2012).
[23] J. Xiao, W. L. Ong, Z. Guo, G. W. Ho, and K. Zeng, ACS Appl. Mater. Inter. **7**, 11412 (2015).
[24] J. Xiao, K. Zeng, L. M. Wong, and S. Wang, J. Mater. Res. **30**, 3431 (2015).
[25] D. A. Bonnell, S. V. Kalinin, A. L. Kholkin, and A. Gruverman, MRS Bull. **34**, 648 (2009).
[26] A. Gruverman, J. Mater. Sci. **44**, 5182 (2009).
[27] S. V. Kalinin, A. N. Morozovska, L. Q. Chen, and B. J. Rodriguez, Rep. Prog. Phys. **73**, 056502 (2010).
[28] J. A. Christman, R. R. Woolcott, A. I. Kingon, and R. J. Nemanich, Appl. Phys. Lett. **73** (1998).
[29] L. P. Schuler, N. Valanoor, P. Miller, I. Guy, R. J. Reeves, and M. M. Alkaisi, J. Electron. Mater. **36**, 507 (2007).
[30] D. A. Scrymgeour, T. L. Sounart, N. C. Simmons, and J. W. P. Hsu, J. Appl. Phys. **101** (2006).
[31] I. K. Bdikin, J. Gracio, R. Ayouchi, R. Schwarz, and A. L. Kholkin, Nanotechnology **21**, 235703 (2010).
[32] M. Laurenti, S. Stassi, M. Lorenzoni, M. Fontana, G. Canavese, V. Cauda, and C. F. Pirri, Nanotechnology **26**, 215704 (2015).
[33] C. Ping and B. H. Yang, Journal of Electronic Materials **40**, 253 (2011).
[34] M. H. Zhao, Z. L. Wang, and S. X. Mao, Nano Lett. **4**, 587 (2004).
[35] K. Momeni, A. Asthana, A. Prasad, Y. K. Yap, and R. Shahbazia-Yassar, Appl. Phys. A **109**, 95 (2012).
[36] B. Bercu, W. Geng, O. Simonetti, S. Kostcheev, C. Sartel, V. Sallet, G. Lerondel, M. Molinari, L. Giraudet, and C. Couteau, Nanotechnology **24**, 415202 (2013).
[37] V. B. Chu, H. D. Cho, T. W. Kang, and W. Yang, Thin Solid Films **520**, 4622 (2012).
[38] S. Kurbanov, W. C. Yang, and T. W. Kang, Appl. Phys. Express **4**, 021101 (2011).
[39] C. Maragliano, S. Lilliu, M. S. Dahlem, M. Chiesa, T. Souier, and M. Stefancich, Sci. Rep. **4**, 4203 (2014).
[40] M. F. Wong, T. S. Herng, Z. Zhang, K. Zeng, and J. Ding, Appl. Phys. Lett. **97**, 232103 (2010).
[41] A. Kumar, T. S. Herng, K. Zeng, and J. Ding, ACS Appl. Mater. Interfaces **4**, 5276 (2012).
[42] A. Di Trolio, P. Alippi, E.M. Bauer, G. Ciatto, M. H. Chu, G. Varvaro, A. Polimeni, M. Capizzi, M. Valentini, F. Bobba, C. Di Giorgio, and A. Amore Bonapasta, ACS Appl. Mater. Interfaces **8**, 12925 (2016).
[43] A. Di Trolio, P. Alippi, G. Ciatto, G. Scavia, M. Valentini, and A. Amore Bonapasta, J. Mater. Chem. C **3**, 10188 (2015).